Indoor UAV Localization Using a Tether

Xuesu Xiao[1], Yiming Fan[2], Jan Dufek[1] and Robin Murphy[1]

***Abstract*— This paper presents an approach to localize a UAV in indoor environments using only a quasi-taut tether. In indoor GPS-denied environments, UAV localization usually depends on vision-based methods combined with inertial sensing, such as visual odometry or SLAM using 2D/3D cameras or laser range finders. This necessitates either heavy and sophisticated sensor payload mounted onto the UAV platform or computationally expensive algorithms running online. In this work, we investigate another indoor localization possibility for a tethered UAV: using the tether's sensory feedback, which is fed into a catenary-based mechanics model, to localize the UAV in an indoor global frame defined by the tether reel center. Our localization method is tested on a physical robot, Fotokite Pro. Our approach could reduce the error of the state-of-the-art tether-based indoor aerial vehicle localization by 31.12%. Since the UAV is localized with respect to the tether reel center, our method could be used to localize the UAV in a moving frame. So it is particularly suitable for inter-localization within marsupial heterogeneous robotic teams for urban search and rescue purposes.**

I. INTRODUCTION

Unmanned Aerial Vehicles (UAVs) have been widely used in an increasing number of areas, including surveillance, search and rescue [1]–[4], post-disaster assessment [5], [6], and nuclear decommissioning. UAV's applications are not limited in outdoor environments, but also cover indoor spaces, which are not favorable for human access, such as collapsed buildings in post-disaster scenarios. For localization, UAVs applied outdoor rely on Global Position System (GPS) and Inertia Measurement Unit (IMU) [7]. Through triangulation with multiple satellites, outdoor UAVs can determine its location in the earth frame. The localization error could be alleviated by integrating IMU information. However, indoor environments are usually GPS-denied. So localization become heavily dependent on inertia and vision [8]–[12]. Inertia sensing is prone to drift since sensor error accumulates over time through integration. Using vision-based methods requires 2D/3D cameras or laser range finders to be mounted onto the UAV platform. Extracting and matching feature points from RGB frames and registering point cloud add large computational overhead to the data processing pipelines. Some vision-based methods are also very sensitive to environmental condition changes, such as environment illumination, background clutteredness, or moving objects. All these problems make indoor UAV localization a challenging task.

[1]Xuesu Xiao, Jan Dufek, and Robin Murphy are with the Department of Computer Science and Engineering, Texas A&M University, College Station, TX 77843 {xiaoxuesu, dufek, robin.r.murphy}@tamu.edu

[2]Yiming Fan is with the Department of Mechanical Engineering, Texas A&M University, College Station, Texas 77843 yimingfan@tamu.edu

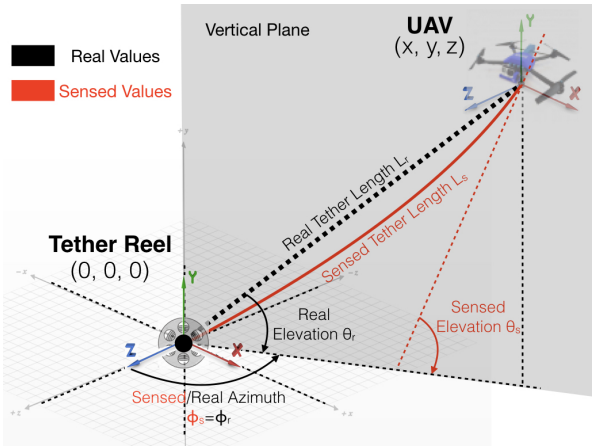

Fig. 1. Tethered UAV is localized using tether-based sensory feedback including tether length, azimuth, and elevation angle. Our preliminary localizer assumes sensed tether length, azimuth, and elevation angles are in fact the real values. In this paper, we looks into this invalid assumption especially with longer tether and compensate the values with a reasonable offset.

In this paper, we propose a new sensor modality for indoor localization of a tethered UAV, which utilizes tether-based feedback to avoid using GPS, inertia, and vision-based sensing. Our UAV localizer uses tether length from tether reel encoder, tether azimuth and elevation angle from tether angle sensor, and then feeds those sensory information into a mechanics model to retrieve configuration of an imaginary absolutely straight tether between the origin (tether reel center) and the UAV (Fig. 1). The computational cost introduced is minimal. This paper assumes an ideal open space, which means there are no obstacles between the UAV and the reel center. To deal with more realistic obstacle-present spaces where tether may contact the environment, the readers are suggested to refer to the tether contact planner discussed in [3].

This paper is organized as follows: Sec. II reviews related work regarding indoor UAV localization and introduces a preliminary version of our tether-based localizer. Sec. III describes the mechanics model we use to quantify the actual deformation of the tether instead of an ideal straight line. Sec. IV gives implementation details of our proposed approach. Sec. V presents experimental results used to show the efficacy of our proposed method and shows improvement in terms of localization accuracy. Sec. VI concludes the paper.

II. Related Work

UAVs have been widely used in after-disaster responses [5], [6]. Urban search and rescue missions push the traditional usage of UAVs in outdoor open spaces with GPS links into indoor cluttered GPS-denied environments. Unlike triangulating signals from multiple satellites orbiting around the globe [7], UAVs flying indoors need to use its proprioceptive sensing to determine its own states. Among those, localization is a crucial part for the following controls, navigation, planning, and higher level autonomy.

Indoor UAV localization is largely dependent on inertia and vision-based methods. Although localization based on IMUs is self-contained and doesn't rely on any interaction with external sources, IMUs are prone to errors due to outside condition changes such as temperature and sensor drift caused by long-term integration. So vision-based methods were developed using camera or laser range finder to localize UAV using RGB and depth information: [8] matched images from a monocular camera and recorded landmark feature points in order to estimate the UAV's location. [9]'s UAV was equipped with stereo camera so the localization could be based on triangulating two different video streams. [10] utilized 3D model of the edges in the environments and used a multiple hypotheses tracker to retrieve the potential poses of the UAV from the observations in the image. [11] augmented the IMU and downward facing mono-camera with a planar laser range finder for localization. Vision-based methods, however, are very sensitive to environmental condition changes, such as illumination, and running vision algorithms is computational expensive. Ultra-WideBand (UWB) technology was developed to help indoor UAV localization [13]. [12] proposed to use UWB technology to further enhance the traditional sensor modalities, including IMU and vision. However, those techniques along with wireless sensor networks [14], [15], infrared [16], RFID [17], assumed localization devices were pre-installed in the environment, which is not applicable for search and rescue scenarios. Different filtering techniques were attempted to improve the localization accuracy based on noisy sensory input [12], [15].

In this paper, we propose a localization technique for tethered UAVs. In the literature, tethered UAVs were not treated differently than its tetherless counterpart [18]. To our best knowledge, there is no research focusing on localization specifically for tethered UAVs. While transmitting power and data plus serving as a failsafe, taut tether could also double as an effective way for localization. In [1]–[3], we used a preliminary tether-based localizer which utilized polar-to-Cartesian coordinates transformation (Fig. 1). The idea was using tether length L_r (from tether reel encoder), tether elevation angle θ_r and azimuth angle ϕ_r (from tether angle sensor), the 3D position of the UAV could be uniquely determined:

$$\begin{cases} x = & L_r cos\theta_r sin\phi_r \\ y = & L_r sin\theta_r \\ z = & L_r cos\theta_r cos\phi_r \end{cases} \tag{1}$$

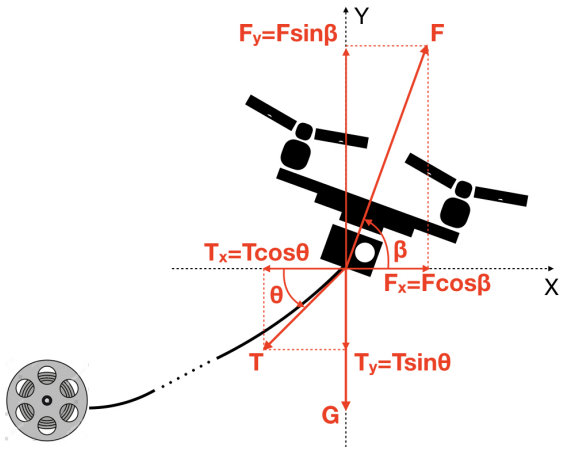

Fig. 2. Free Body Diagram of the Tethered UAV

However, the assumption that the tether is always taut and therefore straight does not hold all the time ($L_r \neq L_s$, $\theta_r \neq \theta_s$), especially when the tether is long and the tether forms an arc instead of a straight line due to increased gravitational force (red part in Fig. 1). So the localization accuracy is deteriorated due to invalid straight tether assumption. The localizer proposed in this paper specifically addresses this problem: we use a mechanics model to compensate the offset in tether length and elevation angle and improve localization accuracy compared to the preliminary localizer.

III. Tether Deformation Model

This section gives a detailed mechanics model we use to quantify the differences in sensed and real tether values. We start with a free body diagram analysis, which calculates the force from tether pulling the UAV down (tether tension) using UAV configuration and sensory feedback. Based on that we further introduce our tether deformation model. The model takes calculated tether tension and sensed elevation angle as input, and output the real elevation angle and tether length.

A. Free Body Diagram

A UAV flying with a taut tether needs to hover with an angle with respect to the horizontal plane since the propellors need to provide a horizontal force to balance the horizontal component of tether tension acting on the UAV. As shown in Fig. 2, we denote the force created by the propellers F, tether tension T, and the gravity of the UAV G. The angles of F and T with respect to the horizontal plane is denoted as β and θ, respectively. θ is simply the sensed elevation angle described above.

To balance both x and y directions, we have

$$\begin{cases} Fcos\beta = Tcos\theta \\ Fsin\beta = Tsin\theta + G \end{cases} \tag{2}$$

β is available from UAV onboard IMU and θ from tether angle sensor. By solving the equations, we can calculate F and T:

$$\begin{cases} F = \frac{G}{sin\beta - tan\theta cos\beta} \\ T = \frac{Gcos\beta}{sin\beta cos\theta - tan\theta cos\theta cos\beta} \end{cases} \tag{3}$$

B. Mechanics Model

In order to describe the shape of the tether, catenary curve is considered. The catenary curve was first introduced by Leibniz, Huygens and Johann Bernoulli in 1691 and it has been widely used in predicting geometric response of hanging ropes, chains and cables under the force of gravity. Assuming the gravity is uniform, and the two free ends of the tether are hanged on the same altitude. Based on symmetry, only half of the catenary is needed for analysis.

Fig. 3a shows the free body diagram of the tether. Point B is the UAV end where the tether is suspended, while point A is the axisymmetric end. The tether is subject to gravity W, which is assumed to be uniformly distributed as shown. The tension acting on the tether is noted as T_0 and T_1, where T_0 is at end A and T_1 at end B. T_1 is the reaction force of T acting on the UAV, as mentioned in the last subsection, so they have same magnitude but opposite directions. By applying equilibrium equations to the tether, we can get:

$$\begin{cases} \Sigma F_x = 0 & \Rightarrow \quad T_1 cos\theta - T_0 = 0 \\ \Sigma F_y = 0 & \Rightarrow \quad T_1 sin\theta - W = 0 \end{cases} \tag{4}$$

where θ is the same departure angle of tension T_1 with respect to the horizontal axis, which we can measure through tether angle sensor. By rewriting Eqn. 4 we have:

$$\begin{cases} T_1 cos\theta &= T_0 \\ T_1 sin\theta &= \rho L g \end{cases} \tag{5}$$

where ρ is the linear density of the tether, g is the gravitational acceleration and L is the total tether length.

A closer look into the free body diagram of one small piece of tether segment is shown in Fig. 3b. The equilibrium equations are:

$$\begin{cases} \Sigma F_x = 0 \Rightarrow & T_{x+\Delta x} cos\theta_{x+\Delta x} - T_x cos\theta_x &= 0 \\ \Sigma F_y = 0 \Rightarrow & T_{x+\Delta x} sin\theta_{x+\Delta x} - T_x sin\theta_x - \Delta W &= 0 \end{cases} \tag{6}$$

where T_x and $T_{x+\Delta x}$ are the tension and θ_x and $\theta_{x+\Delta x}$ the angle with respect to the horizontal axis at both ends of the segment. For the second equation in Eqn. 6, move ΔW to the right hand side and divide both sides by Δx, the left hand side is the definition of derivation of $T_x sin\theta_x$:

$$\frac{d}{dx}(T_x sin\theta_x) = \frac{d}{dx} W_x \tag{7}$$

T_x can be expressed as a function of T_0 and θ_x:

$$T_x = \frac{T_0}{cos\theta_x} \tag{8}$$

The geometry of the tether segment gives us:

$$\begin{cases} dL = \sqrt{d_x^2 + d_y^2} = \sqrt{1 + (\frac{dy}{dx})^2} dx \\ tan\theta_x = \frac{dy}{dx} \end{cases} \tag{9}$$

Substituting T_x in Eqn. 7 with Eqn. 8, we get:

$$\frac{d}{dx}(T_0 tan\theta_x) = \frac{d}{dx} W_x = \rho g dL \tag{10}$$

And by substituting Eqn. 9 into Eqn. 10, we have:

$$\frac{d}{dx}(\frac{dy}{dx}) = \frac{\rho g}{T_0} \sqrt{1 + (\frac{dy}{dx})^2} dx \tag{11}$$

The solution to Eqn. 11 is the catenary curve and can be expressed as:

$$y = a cosh \frac{x}{a} \tag{12}$$

where $a = \frac{T_0}{\rho g}$ is a coefficient that depends on tension T_0, tether linear density ρ, and gravitational acceleration g. In order to get the coordinate of the UAV end, we take the derivative of Eqn. 12:

$$\frac{dy}{dx} = sinh \frac{x}{a} \tag{13}$$

By comparing Eqn. 13 and Eqn. 9, we get:

$$tan\theta_x = sinh \frac{x}{a} \tag{14}$$

Eqn. 14 is a general form and specifically at the UAV end B, θ_x is the departure angle θ, and x coordinate is equal to L_x:

$$tan\theta = sinh \frac{L_x}{a} \tag{15}$$

Based on Eqn. 15 and catenary curve, the x and y coordinates of the UAV end B takes the form:

$$\begin{cases} L_x = & a ln(tan\theta + \sqrt{tan^2\theta + 1}) \\ L_y = & a cosh \frac{L_x}{a} - a cosh 0 \end{cases} \tag{16}$$

The real elevation angle θ_r and tether length L_r would be corrected as:

$$\begin{cases} \theta_r = & atan(\frac{L_y}{L_x}) \\ L_r = & \sqrt{L_x^2 + L_y^2} \end{cases} \tag{17}$$

while real azimuth angle ϕ_r is still equal to sensed value ϕ_s. Using arc length equation, we could compute the actual length of the curved tether S:

$$\begin{aligned} S &= \int_0^{L_x} \sqrt{1 + f'(x)^2} dx \\ &= \int_0^{L_x} \sqrt{1 + sinh^2 \frac{x}{a}} dx \\ &= a sinh \frac{L_x}{a} \end{aligned} \tag{18}$$

IV. Implementation

This section gives details about the implementation of our proposed localization method. We use a physical robot, Fotokite Pro, with its provided Software Development Kit (SDK) to implement our approach.

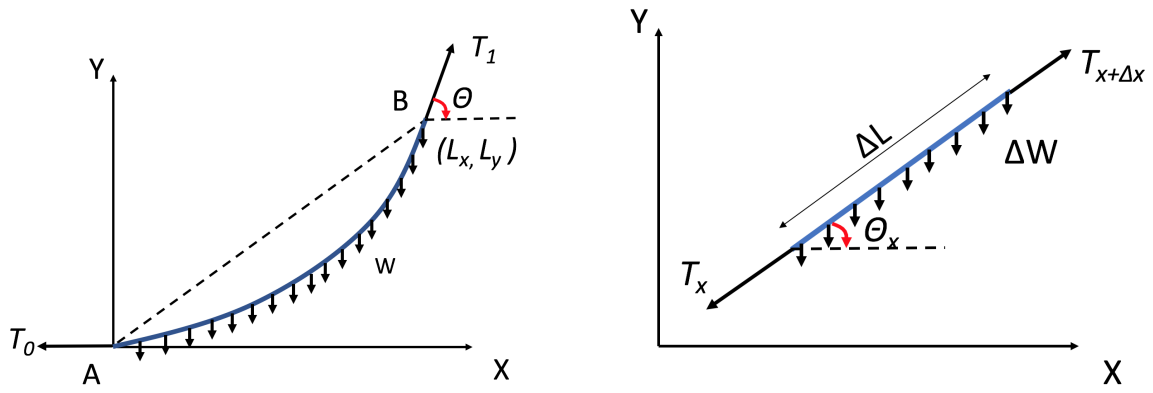

(a) Free Body Diagram of UAV Tether

(b) Free Body Diagram of Tether Segment

Fig. 3. Free Body Diagram of the Entire Tether and One Piece Tether Segment: both experience tension from two ends and uniformly distributed gravity

A. Sensory Input

1) Tether Length L_s: Using the encoder reading of the tether reel from the SDK, we are able to calculate the relative tether length with respect to its initial state. If we initialize tether length to be zero, the absolute tether length equals to the relative value.

2) Tether Angles θ_s and ϕ_s: The SDK also provides two tether angle measurements, azimuth and elevation, measured directly from the attachment point of the tether to the vehicle. Elevation angle is with respect to gravity and azimuth to initialization. We convert the elevation angle based on our definition with respect to horizontal plane.

3) Vehicular Lean Angle β: The UAV configuration is given in the form of a quaternion $\mathbf{z} = \mathbf{a} + \mathbf{bi} + \mathbf{cj} + \mathbf{dk}$. The normal vector pointing up $\mathbf{n_v} = [\mathbf{0}, \mathbf{1}, \mathbf{0}]^\mathbf{T}$ expressed in the vehicle frame could be transformed to the global frame by multiplying the corresponding rotation matrix R of the quaternion:

$$n_g = [x_g, y_g, z_g]^T = R * n_v \tag{19}$$

So the lean angle is

$$\beta = arcsin(\frac{y_g}{\sqrt{x_g^2 + y_g^2 + z_g^2}}) \tag{20}$$

B. Length and Angle Correction

We take the sensed elevation angle θ_s and computed lean angle β to compute tension $T = T_0$ using Eqn. 3. Here the UAV weighs 6N. Then we feed them into the model described in Sec. III. Tether linear density ρ is measured to be 0.0061kg/m. Eqn. 17 gives the final corrected elevation angle θ_r. The control for tether length need to be based on the arc length S (Eqn. 18). Azimuth angle remains the same.

C. Navigation

In order to navigate the UAV to target point (x, y, z), we compute the desired elevation θ_d and azimuth ϕ_d values by:

$$\begin{cases} \theta_d = & arcsin(\frac{y}{\sqrt{x^2+y^2+z^2}}) \\ \phi_d = & atan2(\frac{x}{z}) \end{cases} \tag{21}$$

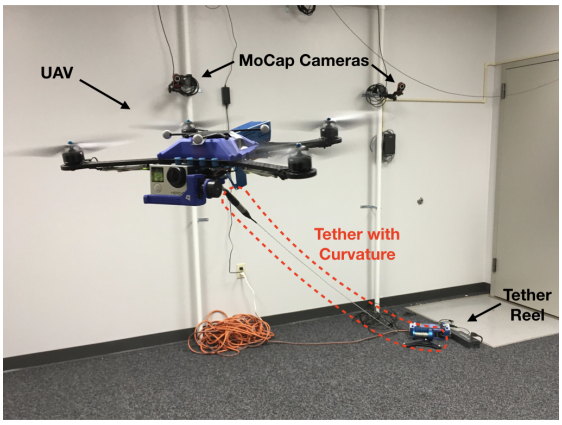

Fig. 4. Experimental Setup: UAV flying in a motion capture studio with a tether pulled down by gravity

The desired tether arc length L_d is given by Eqn. 18. By comparing the desired values with corrected current sensory input, three individual PID controllers are implemented to drive L_r, θ_r, and ϕ_r to their desired values.

V. Experiments

In order to show the efficacy of our proposed approach, we conduct experiments in a motion capture studio to capture motion ground truth (Fig. 4). The studio is equipped with 12 OptiTrack Flex 13 cameras running at 120 Hz. The 1280×1024 high resolution cameras with a 56° Field of View provide less than 0.3mm positional error and cover the whole 2.5×2.5×2.5m space.

Since our approach does not affect azimuth angle, we fix the experiments at a constant azimuth. All experiment points are chosen on a horizontal plane with -45°azimuth angle (Fig. 5 left). Within this plane, points are located on a grid pattern with an interval of 0.5m (Fig. 5 right). We fly the UAV, Fotokite Pro, to and hover at each individual experiment points, using the preliminary and our proposed localizer. Ground truth positional data is recorded by the motion capture system.

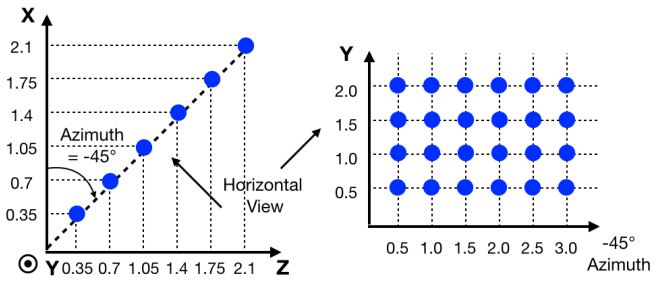

Fig. 5. Experimental points are chosen within a horizontal plane with -45°azimuth angle. Within this plane, points are distributed over a grid with 0.5m interval.

48 localization trials are performed with 48 ground truth positions collected, 24 using preliminary localizer and the other 24 our new approach. Due to the turbulence created by the propellors in a confined indoor studio space, the UAV wobbles at the target location. So for each data point, we record the motion of Fotokite as a rigid body using the motion capture system for 5 seconds after it stabilizes at the target location. Average value is taken over the 600 tracked points (5 seconds at 120 Hz). All 48 localized points along with the 24 target points from our physical experiments are displayed in Fig. 6. While blue points designate the ideal target points where the UAV should localize and hover at, red and green points denote localization results from the preliminary and our proposed localizer, respectively. Red and green straight line segments illustrate the correspondence between localization results and target point.

As Fig. 6a shows, green straight line segments are usually shorter than the red ones connected with the same blue points. This means improved localization accuracy using our proposed localizer. A closer look into the experimental results are shown in Fig. 6b and 6c. Fig. 6b is the perpendicular view toward -45°azimuth plane. It could be observed that red points are always lower than blue points. This is the reason caused by the invalid straight tether assumption (Fig. 1). The real elevation angle is always smaller than the sensed value, so given a certain tether length the preliminary localizer thinks the UAV were at a higher position, but in fact it's lower. Green points achieved by our new model are distributed around blue points, with a smaller distance. This shows that our proposed localizer overcomes the problem caused by invalid straight tether assumption and reduces the localization error in the vertical direction. Fig. 6c shows the top town view of the 48 trials and directly illustrate the localization accuracy in the horizontal plane. There is not much difference to be observed between red and green points with respect to the blue ones since our localizer doesn't deal with azimuth angle correction. The slightly denser distribution within 0 and -45°is due to tether azimuth and vehicular yaw angle initialization error. Overall speaking, the improvement of localization accuracy is summarized in Tab. I.

As mentioned in Sec. II, accuracy of the preliminary localizer is deteriorated with increasing tether length. Fig. 7 looks into this effect in detail. In general, localization error from the preliminary localizer is worse (red points) than our proposed method (green points). A line is fitted to the results of each localizer using linear regression. As we can see, the red line indicates that longer tether length has a significant negative effect on localization accuracy, while our proposed method is not sensitive to increasing tether length. Our proposed localizer has a limited average localization error within 0.4m. This is the best hovering stability achievable by Fotokite's built-in controller measured by experiments [3].

TABLE I
AVERAGE TRACKING ERROR

	Preliminary Localizer	Proposed Method	Improvement
Average Localization Error (m)	0.5335	0.3675	31.12%

VI. CONCLUSION

In this paper, we present a novel indoor localization scheme for UAVs operating with a quasi-straight tether. This localizer is based on polar-to-Cartesian coordinates conversion and uses tether sensory information including tether length, elevation and azimuth angles. More importantly, a mechanics model is built to quantify the inevitable tether deformation when the tether is long and pulled down by gravity and therefore forming an arc instead of an ideal straight line. This model is capable of correcting the measured elevation angle and tether length and thus improve localization accuracy. The improved localization accuracy is demonstrated by experiments on a physical tethered UAV, Fotokite Pro. The results indicate that our model is able to ameliorate localization accuracy by 31.12% and effectively eliminate the negative effect of increased tether length on localization result. The average localization error achieved by our proposed method is limited within the hovering stability tolerance of our particular UAV platform.

In future work, more sophisticated mechanics model will be used to further improve the tracking accuracy, such as Finite Element Analysis. Machine learning approaches are another research direction to model the mapping from UAV tether's sensory feedback to UAV's global position. For example, Deep Neural Networks could be trained using tether sensor values and ground truth position collected by motion capture system. This catenary-based localizer will be embedded into a marsupial heterogeneous robotic team for urban search and rescue purposes including a primary ground robot and the UAV in order to improve the tethered UAV's higher level state estimation, controls, navigation, planning, and autonomy.

ACKNOWLEDGMENT

This work is supported by NSF grant IIS 1426756, DOE Science of Safety Grant 1710670, and DOE DE-EM0004483.

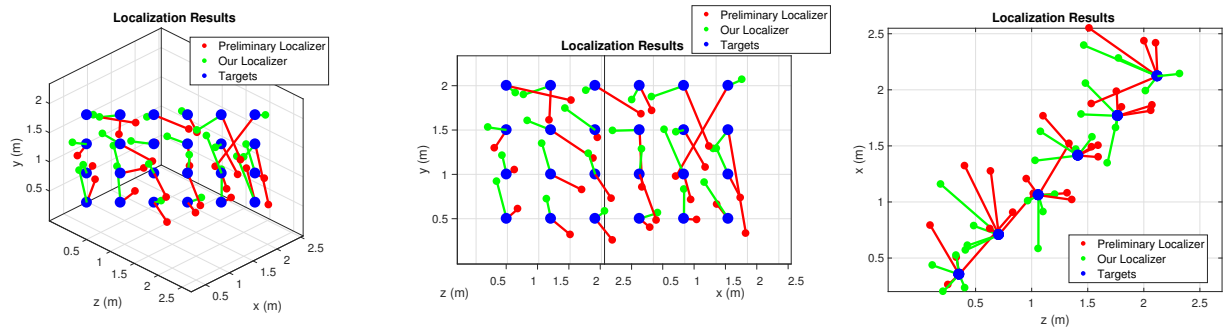

(a) 3-D Illustration of Experimental Results (b) -45° Azimuth Plane Horizontal View (c) Top Down View

Fig. 6. Localization Results from 48 Experimental Trials: blue points designate the target points the UAV should localize and hover at. Red points are the localization results using the preliminary localizer. Green points are resulted by our proposed mechanics-based approach. Small straight line segments connect localization results with their corresponding targets.

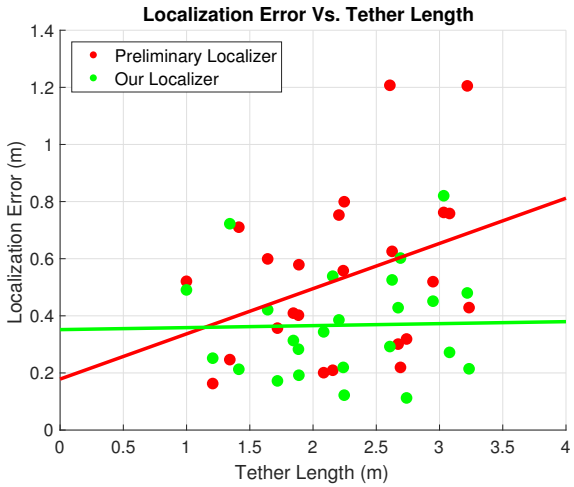

Fig. 7. Localization Error in Terms of Tether Length: Preliminary localizer's error (red) increases with longer tether, while tether length does not have a significant effect on our proposed method (green).

The authors would like to thank Mohamed Suhail for his help with the motion capture system.

REFERENCES

[1] X. Xiao, J. Dufek, and R. Murphy, "Visual servoing for teleoperation using a tethered uav," in *Safety, Security and Rescue Robotics (SSRR), 2017 IEEE International Symposium on*. IEEE, 2017.

[2] J. Dufek, X. Xiao, and R. Murphy, "Visual pose stabilization of tethered small unmanned aerial system to assist drowning victim recovery," in *Safety, Security and Rescue Robotics (SSRR), 2017 IEEE International Symposium on*. IEEE, 2017, pp. 116–122.

[3] X. Xiao, J. Dufek, and R. Murphy, "Motion planning for a uav with a straight or kinked tether," in *Intelligent Robots and Systems (IROS), 2018 IEEE/RSJ International Conference on*. IEEE, 2018.

[4] X. Xiao, J. Dufek, T. Woodbury, and R. Murphy, "Uav assisted usv visual navigation for marine mass casualty incident response," in *Intelligent Robots and Systems (IROS), 2017 IEEE/RSJ International Conference on*. IEEE, 2017, pp. 6105–6110.

[5] K. S. Pratt, R. R. Murphy, J. L. Burke, J. Craighead, C. Griffin, and S. Stover, "Use of tethered small unmanned aerial system at berkman plaza ii collapse," in *Safety, Security and Rescue Robotics, 2008. SSRR 2008. IEEE International Workshop on*. IEEE, 2008, pp. 134–139.

[6] R. Murphy, J. Dufek, T. Sarmiento, G. Wilde, X. Xiao, J. Braun, L. Mullen, R. Smith, S. Allred, J. Adams *et al.*, "Two case studies and gaps analysis of flood assessment for emergency management with small unmanned aerial systems," in *Safety, Security, and Rescue Robotics (SSRR), 2016 IEEE International Symposium on*. IEEE, 2016, pp. 54–61.

[7] A. Nemra and N. Aouf, "Robust ins/gps sensor fusion for uav localization using sdre nonlinear filtering," *IEEE Sensors Journal*, vol. 10, no. 4, pp. 789–798, 2010.

[8] J.-O. Lee, T. Kang, K.-H. Lee, S. K. Im, and J. Park, "Vision-based indoor localization for unmanned aerial vehicles," *Journal of Aerospace Engineering*, vol. 24, no. 3, pp. 373–377, 2010.

[9] S. Azrad, M. Fadhil, F. Kendoul, and K. Nonami, "Quadrotor uav indoor localization using embedded stereo camera," in *Applied Mechanics and Materials*, vol. 629. Trans Tech Publ, 2014, pp. 270–277.

[10] C. Teuliere, E. Marchand, and L. Eck, "3-d model-based tracking for uav indoor localization," *IEEE Transactions on cybernetics*, vol. 45, no. 5, pp. 869–879, 2015.

[11] F. Wang, J. Cui, S. K. Phang, B. M. Chen, and T. H. Lee, "A mono-camera and scanning laser range finder based uav indoor navigation system," in *Unmanned Aircraft Systems (ICUAS), 2013 International Conference on*. IEEE, 2013, pp. 694–701.

[12] A. Benini, A. Mancini, and S. Longhi, "An imu/uwb/vision-based extended kalman filter for mini-uav localization in indoor environment using 802.15. 4a wireless sensor network," *Journal of Intelligent & Robotic Systems*, vol. 70, no. 1-4, pp. 461–476, 2013.

[13] J. Tiemann, F. Schweikowski, and C. Wietfeld, "Design of an uwb indoor-positioning system for uav navigation in gnss-denied environments," in *Indoor Positioning and Indoor Navigation (IPIN), 2015 International Conference on*. IEEE, 2015, pp. 1–7.

[14] J. L. Rullan-Lara, G. Sanahuja, R. Lozano, S. Salazar, R. Garcia-Hernandez, and J. A. Ruz-Hernandez, "Indoor localization of a quadrotor based on wsn: a real-time application," *International Journal of Advanced Robotic Systems*, vol. 10, no. 1, p. 48, 2013.

[15] J.-L. Rullán-Lara, S. Salazar, and R. Lozano, "Real-time localization of an uav using kalman filter and a wireless sensor network," *Journal of Intelligent & Robotic Systems*, vol. 65, no. 1-4, pp. 283–293, 2012.

[16] N. Kirchner and T. Furukawa, "Infrared localisation for indoor uavs," in *Proc. of the 1st Int. Conf. on Sensing Technology*, 2005.

[17] J. S. Choi, B. R. Son, H. K. Kang, and D. H. Lee, "Indoor localization of unmanned aerial vehicle based on passive uhf rfid systems," in *Ubiquitous Robots and Ambient Intelligence (URAI), 2012 9th International Conference on*. IEEE, 2012, pp. 188–189.

[18] L. Zikou, C. Papachristos, and A. Tzes, "The power-over-tether system for powering small uavs: tethering-line tension control synthesis," in *Control and Automation (MED), 2015 23th Mediterranean Conference on*. IEEE, 2015, pp. 681–687.